NDT.net
ReJNDT

Virtual encoder: a two-dimension visual odometer for NDT

Thiago E. Kalid[1], Everton Trento Jr[1], Tatiana A. Prado[1], Gustavo P. Pires[2], Giovanni A. Guarneri[1], Thiago A. R. Passarin[1] and Daniel R. Pipa
1 Federal University of Technology - Parana, Brazil, passarin@utfpr.edu.br
2 Petrobras Research Center, Brazil, gustavopires@petrobras.com.br

More info about this article: https://www.ndt.net/?id=28119

Abstract

Odometer information is an important feature of NDT systems for inspection procedures that involve mechanical scanning. Knowledge of transducer position during the inspection allows for the localization of flaws and the fusion (stitching) of several images into more sophisticated representations of the inspected object. Commercial encoders provide NDT systems with accurate real-time displacement information that can be integrated to obtain odometry. However, this information is typically limited to a single axis. Although composite schemes with more than one encoder can be built to provide 2-D or 3-D spatial information, they are mechanically intricate and lack flexibility and ease of use. We propose a 2-D position-tracking solution that is based on image processing. A miniature camera continuously captures images of the external surface of the inspected object, which are fed to an algorithm that detects and stores 2-D displacement between each pair of consecutive images. Additionally, the orientation quaternions provided by an Inertial Measurement Unit are stored, allowing for posterior 3-D path reconstruction over objects of known geometries, such as oil pipes. Besides logging position and orientation histories, the device also provides real-time displacement information to the NDT system, where it is perceived as a set of single-axis encoders, thus termed “the virtual encoder”. We demonstrate the applicability of the device to both contact and immersion ultrasonic inspections. The results show that the concept is promising, despite being based on simple principles and relatively easy to implement. The source code is provided as additional material in https://github.com/thiagokalid/Virtual-Encoder-ECNDT-2023.

KEYWORDS: Visual-odometry; Motion estimation; Downward-facing camera; Nondestructive testing

© 2023 The Authors. Published by NDT.net under License CC-BY-4.0 https://creativecommons.org/licenses/by/4.0/ https://doi.org/10.58286/28119

1. Introduction

Many nondestructive testing (NDT) routines involve mechanical sweeping of the probes. An example is ultrasound (US) imaging of regions larger than the width of the probe active aperture, e.g., [1]. Stitching multiple images is necessary in these cases to form a significant representation. Wheel encoders usually accomplish the task if the sweeping is restrained to one dimension. For two-dimensional (2-D) displacements, however, the use of wheel encoders results in large and complicated schemes (see, for instance, the Zetec NDT Sweeper™).

Downward-facing cameras have been demonstrated as simple and versatile sensors for 2-D visual odometry systems [2, 3]. These systems measure global motion between each pair of consecutive frames using phase correlation methods (PCM) [4]. These methods take only the phase information of the images into account, being insensitive to image content and robust to noise and corruption [4].

In the work herein reported, the same concept of a downward-facing camera was applied to 2-D odometry for NDT. The application we aim at is ultrasound imaging of steel pipes, where displacements in axial and longitudinal directions are usually required. The fact that pipes with curved geometries are common motivated the addition of an Inertial Measurement Unit (IMU) to the proposed solution, which provides real-time orientation quaternions, allowing for three-dimensional (3-D) reconstruction of the path performed by the probe.

2. Proposed solution

2.1 System structure

The system and its integration with the US acquisition system are summarized in Fig. 1. The camera provides image frames to the Central Processing Unit (CPU). At instant n, the CPU performs the phase correlation (PC) of frames $n-1$ and n to estimate the n-th 2-D displacement, which is sent to the Pulser Module through Ethernet and stored in the local memory. The instantaneous orientation quaternion for instant n, provided by the IMU, is stored as well. Upon reception, the Pulser Module immediately emulates the Transistor-Transitor Logic (TTL) pulses that would be fired by wheel encoders for the n-th 2-D displacement. The US acquisition system receives the TTL pulses through the encoder input, interprets as if they were generated by a wheel encoders fixed at the probe and

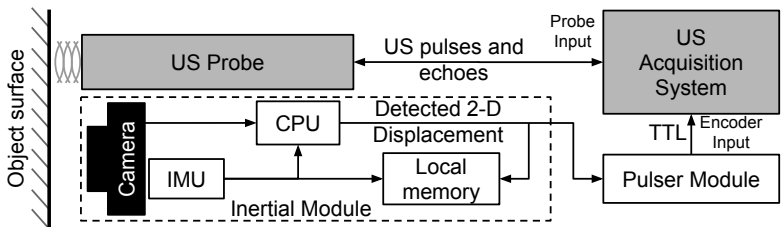

Figure 1. System architecture.

fires the US probe according to user-defined configuration. The received US echoes doesn't affect the 2-D displacement estimation. The camera and IMU are mechanically fixed to the US probe.

2.2 Phase Correlation Algorithm

Our implementation of the PC algorithm is based on the frequency-domain subspace identification method proposed in [5]. This family of methods (i.e., frequency-domain) substantially outperforms the classical time-domain PCM in terms of accuracy and robustness to noise [4]. In the following paragraphs, we briefly describe the formulation of our implementation. All the steps are summarized in Fig. 2.

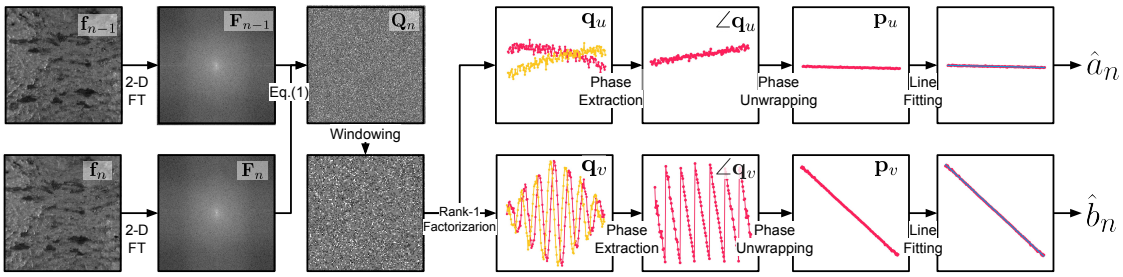

Figure 2. Steps performed for obtainment of the 2-D displacement estimate $(\hat{a}_n, \hat{b}_n)$ from two consecutive frames $\mathbf{f}_{n-1}$ and $\mathbf{f}_n$. The space-domain windowing operations are not explicitly represented.

Let $f_{n-1}(x,y)$ and $f_n(x,y)$ be two consecutive frames captured by the camera, with $F_{n-1} = F_{n-1}(u,v)$ and $F_n = F_n(u,v)$ being their respective Fourier spectra. The two-dimensional global displacement between the frames can be estimated upon the assumption that f_n is a shifted copy of f_{n-1}, i.e., that $f_n(x,y) = f_{n-1}(x-a, y-b)$, where a and b are the horizontal and vertical displacements, respectively, and are measured in pixels. This assumption implies that $f_n = f_{n-1} * \delta(x-a, y-b)$, where $*$ denotes the 2-D convolution and $\delta(x,y)$ is the Dirac delta. Then, the *phase correlation* spectrum Q_n is defined as

$$Q(u,v) = \mathcal{F}\{\delta(x-a_n, y-b_n)\} = \frac{F_{n-1} \odot F_n^*}{|F_{n-1} \odot F_n^*|} = \exp\{-j(ua_n + vb_n)\} \tag{1}$$

where $\mathcal{F}\{\cdot\}$ denotes the 2-D Fourier Transform (FT), $F_n = F_n(u,v) = \mathcal{F}\{f_n(x,y)\}$ is the Fourier spectrum of f_n, F_n^* is the complex conjugate of F_n, and $\odot$ denotes the Hadamard product (entry-wise product). The subspace identification method takes advantage of the fact that the complex exponential of Eq. (1) can be factorized as

$$\exp\{-j(ua_n + vb_n)\} = q_u(u,v)q_v(u,v) = \exp\{-jua_n\}\exp\{-jvb_n\}, \tag{2}$$

where $q_u(u,v) = \exp\{-jua\}$ varies only in the u direction, and $q_v(u,v) = \exp\{-jvb\}$ varies only in the v direction. That means Q_n is rank-one. We now define $\mathbf{Q}_n \in \mathbb{C}^{M\times N}$ as a matrix representation of Q_n, with M and N being the number of lines and columns, respectively. It follows that $\mathbf{Q}_n$ is a rank-one matrix that can be factorized as

$$\mathbf{Q}_n = \mathbf{q}_u \mathbf{q}_v^H, \tag{3}$$

where $\mathbf{q}_u \in \mathbb{C}^M$ and $\mathbf{q}_v \in \mathbb{C}^N$ are column-vectors corresponding to $q_u(u,v)$ and $q_v(u,v)$ respectively, and $\mathbf{q}_v^H$ is the Hermitian transpose of $\mathbf{q}_v$. For an arbitrary $\mathbf{Q}_n$ obtained from noisy and corrupted data, $\mathbf{q}_u$ and $\mathbf{q}_v$ are defined through the Eckart-Young theorem and can thus be obtained via singular value decomposition (SVD) of $\mathbf{Q}_n$ followed by rank-one truncation [5]. The space-domain displacements a and b are encoded in the *phases* of the complex exponentials contained in $\mathbf{q}_u$ and $\mathbf{q}_v$, respectively. We extract the phases with the entry-wise *angle* operator $\angle$:

$$\mathbf{p}_u = \text{unwrap}(\angle \mathbf{q}_u), \tag{4a}$$

$$\mathbf{p}_v = \text{unwrap}(\angle \mathbf{q}_v). \tag{4b}$$

The function unwrap$(\cdot)$ performs the *phase unwrapping* operation, which is necessary since the values of $\angle \mathbf{q}_u$ and $\angle \mathbf{q}_v$ are restricted to the interval $[-\pi, \pi)$ [5]. After phase unwrapping, the entries of $\mathbf{p}_u$ and $\mathbf{p}_v$ should lie over lines with slopes determined by the displacements a and b respectively. These entries are then least squares-fitted to lines to obtain the estimates $\hat{a}_n$ and $\hat{b}_n$. Before the 2-D FT, the frames undergo space-domain windowing to reduce edging effects. Also, before the unit-rank factorization of Eq. (3) through SVD, a windowing of $\mathbf{Q}_n$ is performed to exclude high frequency-components, that tend to be corrupted [5].

2.3 Three-dimensional trajectory

At the n-th frame, the 3-D position (relative to the initial position) $\mathbf{r}_n$ is computed as

$$\mathbf{r}_n = \mathbf{r}_{n-1} + \mathbf{d}_n, \tag{5}$$

where $\mathbf{d}_n$ is the 3-D projection of the 2-D displacement $[\hat{a}_n, \hat{b}_n]^T$, obtained from the current orientation quaternion provided by the IMU.

3. Experiments and Results

An inertial module prototype was encased in a sealed container with a transparent acrylic front for the experiments. Adjustable bolts were used to maintain optimal distance between the camera and the object surface for appropriate focus. A macro lens was placed in front of the camera. Raspberry Pi 4 single board computers (SBC) were used for the implementations of both the CPU and the Pulser Module and were linked to each other via Ethernet. All code was written in Python 3 language. The factorization of Eq. (3) was performed using Scipy SVDS implementation. The IMU and camera are model BNO055 and Raspberry Pi Noir V2, respectively. A 60 Hz frame rate was used to facilitate the generation of complementary material (synchronization with video of the experiment), but the setup allowed up to 140 Hz. Fig. 3a shows a perspective view of the inertial module.

Two template frames were built to restrict the movements within known distances and trajectories: planar and cylindrical. The planar frame allows for excursions of 358.0 mm per 200.3 mm in the horizontal and vertical directions

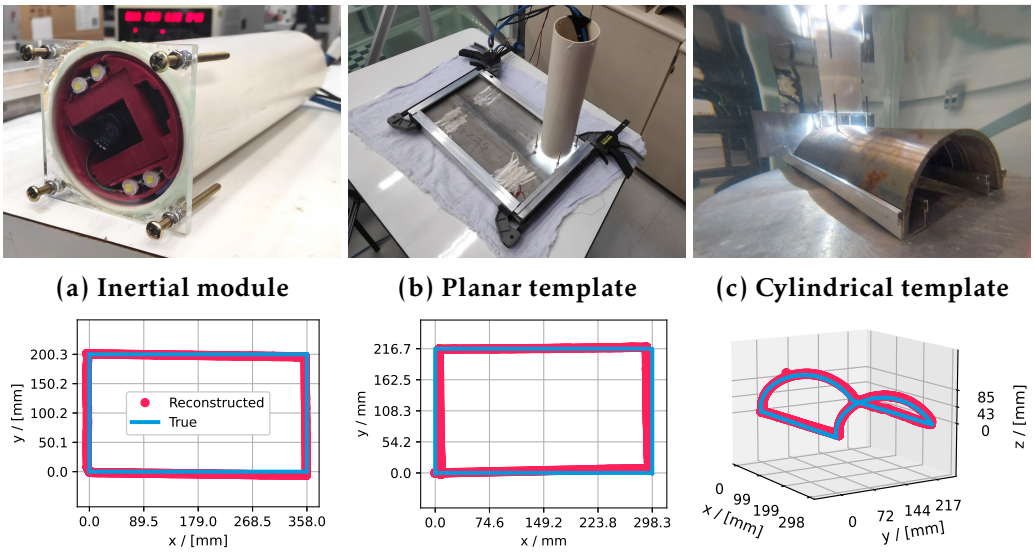

(a) Inertial module **(b) Planar template** **(c) Cylindrical template**

(d) Planar path (2-D) **(e) Cylindrical path (2-D)** **(f) Cylindrical path (3-D)**

Figure 3. Overview of the proposed tests template and its estimated paths.

(Fig. 3b). The cylindrical template allows for 298.3 mm and 216.7 mm excursions in the longitudinal and circumferential directions (Fig. 3c). With a cylinder radius of 85 mm, the circumferential excursion corresponds to 99.6 degrees.

Two types of tests were devised: The first one is a complete closed-loop excursion along the inner borders of the frames, and the second is a one-way, single-direction excursion along one of the inner borders of the frame. The tests were performed in a dry environment (representing US contact inspection) and underwater (representing US immersion inspection).

Cumulative displacements were overall more accurate in contact than immersion scenario (Table 1). This pattern might be related to: lower image distortion, fewer particles in suspension, more uniform scene illumination and better maneuverability due to higher friction between the bolts and the specimen. Maximum error was 12.2 mm or 2.8 % of the traveled distance (in closed-loop the traveled distance is two times the allowed excursion distance for the given axis).

The whole closed-loop reconstructed 2-D paths for the planar frame (contact)

Table 1. Cumulative displacements, in millimeters, measured for the 2-D trajectories reconstructed from the data provided by the virtual encoder.

Test type	Axis	Planar			Cylindrical		
		True	Contact	Immersion	True	Contact	Immersion
Single-x	x	358.0	358.9	357.8	298.3	1,0	-5,34
	y	0.0	-4,7	-7,1	0.0	0,4	-8,4
Single-y	x	0.0	-2,6	-2,5	0.0	1,6	-0,3
	y	200.3	200.7	200.6	216.6	216.5	210.5
Closed loop	x	0.0	-3,4	-3,8	0.0	-1,6	8,2
	y	0.0	7,2	5,5	0.00	5,6	12,2

and the cylindrical frame (immersion) are shown in Fig. 3d and 3e. Fig. 3f shows the 3-D path reconstruction obtained from the fusion of the 2-D cylindrical path with the orientation quaternions provided by the IMU via the iterative application of Eq. (5).

4. Conclusions

A 2-D visual odometer for NDT was proposed and demonstrated to work for both contact and immersion US inspections. The prototype could provide real-time 2-D encoder signaling, which allowed it to be interpreted as a pair of single-axis encoders. Reconstruction of the 3-D path around a cylindrical geometry was also demonstrated as possible. Relative cumulative displacements error were at most 2.8 %, showing that visual-odometry could be part of a reliable 2-D ultrasound odometry system.

Acknowledgements

The authors acknowledge the financial support from PETROBRAS/CENPES through project AUSPEX, CNPq through grant 316234/2021-4, and CAPES - Finance Code 001. The authors also would like to thank UTFPR, Fundação Araucária and FINEP.

References

1. HL de Moura, TA Prado, GA Guarneri, TAR Passarin, D Rossato, GP Pires and DR Pipa, "Surface Estimation via Analysis Method: A Constrained Inverse Problem Approach", IEEE Transactions on Ultrasonics, Ferroelectrics, and Frequency Control, 68(11), pp 3386–3395, DOI: 10.1109/TUFFC.2021.3088013, 2021.
2. M Birem, R Kleihorst and N El-Ghouti, "Visual odometry based on the Fourier transform using a monocular ground-facing camera", Journal of Real-Time Image Processing, 14(3), pp 637–646, DOI: 10.1007/s11554-017-0706-3, 2018.
3. N Nourani-Vatani and PVK Borges, "Correlation-based visual odometry for ground vehicles", Journal of Field Robotics, 28(5), pp 742–768, DOI: 10.1002/rob.20407, 2011.
4. X Tong, Z Ye, Y Xu, S Gao, H Xie, Q Du, S Liu, X Xu, S Liu, K Luan, et al., "Image registration with Fourier-based image correlation: A comprehensive review of developments and applications", IEEE Journal of Selected Topics in Applied Earth Observations and Remote Sensing, 12(10), pp 4062–4081, DOI: 10.1109/JSTARS.2019.2937690, 2019.
5. WS Hoge, "A subspace identification extension to the phase correlation method [MRI application]", IEEE transactions on medical imaging, 22(2), pp 277–280, DOI: 10.1109/TMI.2002.808359, 2003.